Zero : Jurnal Sains, Matematika, dan Terapan
E-ISSN : 2580-5754; P-ISSN : 2580-569X
Volume 10, Number 2, 2026
DOI: 10.30829/zero.v10i2.28088
Page: 831-840

Convergence and Runtime of Crank-Nicolson Schemes for Barrier Option Pricing under Mixed Fractional Brownian Motion

[1]Chatarina Enny Murwaningtyas
Department of Mathematics Education, Sanata Dharma University, Yogyakarta, 55281 Indonesia

Article Info

Article history:

Accepted: 30 August 2026

Keywords:

Barrier Option;
Crank-Nicolson;
Finite-difference;
Mixed Fractional Brownian Motion;
Rannacher Start-up;

ABSTRACT

We examined an up-and-out barrier call under mixed fractional Brownian motion using three finite-difference time integrators: implicit Backward Euler, Crank-Nicolson (CN), and CN with a Rannacher startup. The spatial mesh was kept unchanged, while the number of time steps was increased. CN eventually produced very small price errors, but on course and moderate grids it also produced oscillations and negative values; the effect was stronger at higher volatility. Backward Euler did not show these large undershoots, although its error decreased more slowly. The Rannacher version removed the undershoots in the cases tested with little additional runtime. At $N_t = 128$, its relative error ranged from 8.20×10^{-5} to 1.28×10^{-4}. For this numerical setting, the startup damping gave the most reliable moderate-grid behavior.

Corresponding Author:

Chatarina Enny Murwaningtyas,
Department of Mathematics Education
Universitas Sanata Dharma, Yogyakarta, Indonesia
Email: enny@usd.ac.id

1. INTRODUCTION

For an up-and-out call, most of the numerical difficulty is concentrated at two locations. The terminal payoff changes slope at the strike, while the option value is forced to zero at the upper barrier. Both features have to be represented on the finite-difference grid. Earlier studies discuss the associated boundary and monitoring issues from probabilistic and PDE viewpoints [1], [2], [3], [4]. Ballestra [5] also found that the placement of grid points near the strike and barrier can alter the computed price.

Computation time is included because the same contract may have to be priced repeatedly, as happens in calibration or sensitivity calculations. A scheme can have excellent fine-grid accuracy and still be inconvenient if that accuracy appears only after a very large number of time steps. We therefore report wall-clock time together with min(U), with particular attention to moderate time grids.

The MFBM specification is used here to provide the numerical setting; it is not fitted to a particular market data set. Ordinary Brownian motion has no long-range dependence, whereas FBM introduces self-similarity and long memory [6], [7]. The difficulty with pure FBM is that it is not a semimartingale [8], [9]. Adding an ordinary Brownian component gives the mixed model and, for the Hurst range used here, restores the semimartingale property [10], [11]. Previous MFBM computations report that changes in H and in the mixed diffusion term affect prices as well as numerical convergence [12], [13]. Other studies have considered transaction costs, jumps, and non-standard barriers [14], [15], [16], [17], [18].

Crank-Nicolson has second-order temporal accuracy when the solution is sufficiently smooth, but the present terminal data are not smooth at K. The absorbing upper boundary introduces another abrupt feature. With a coarse time discretization, these two features can produce oscillations and even negative numerical values [19], [20], [21]. Rannacher smoothing changes only the beginning of the calculation: several Backward Euler half steps are taken before the method returns to CN [22], [23]. The comparison here focuses on whether this short initial treatment changes the behavior seen on moderate time grids.

The papers cited above address barrier pricing under MFBM, the convergence of Crank-Nicolson, or remedies for nonsmooth option data. Much less is reported about the combination that matters here: how standard CN and Rannacher-started CN behave under MFBM before the grid is very fine, when price error, negative undershoots, and runtime are considered together. That is the gap examined in this paper. For context, MFBM option pricing has previously been studied for Indonesian options [12]; however, the present parameter set is deliberately controlled and is not calibrated to Indonesian market data.

We compare three time-stepping schemes for the same up-and-out call problem: implicit Backward Euler (IMPL), standard Crank-Nicolson (CN), and Crank-Nicolson with Rannacher start-up (CN-R). The time grid is successively refined while the spatial grid is kept fixed. For each run, we record the price error relative to a fine-grid benchmark, the smallest value attained anywhere in the numerical solution, and wall-clock time. These quantities show not only which method becomes accurate, but also whether it remains numerically admissible while doing so.

2. RESEARCH METHOD

This research is a computational study that evaluates three main aspects: (i) time convergence, (ii) global numerical stability (especially non-negativity), and (iii) computational efficiency across three finite-difference schemes for the valuation of up-and-out barrier call options under the MFBM model. The evaluation is placed in an arbitrage-free framework, so the numerical solution must respect fundamental option-price properties, including non-negative values for non-negative payoffs [24].

The underlying asset S_t is modeled by mixed fractional Brownian motion, a linear combination of standard Brownian motion W_t and independent fractional Brownian motion B_t^H. Under the risk-neutral measure, the asset dynamics are given in Equation (1):

$$dS_t = rS_t\,dt + \alpha\sigma S_t\,dW_t + \beta\sigma S_t\,dB_t^H, \qquad t \in [0,T],\ S_0 > 0, \tag{1}$$

where r is the risk-free interest rate, σ is the volatility scale, and α, β are the weights of the classical and fractional components. In the numerical experiments, we set $\alpha = \beta = 1$ and use $H = 0.85\ (> 3/4)$ to be consistent with the semimartingale conditions in MFBM [8], [10]. Under this condition, the mixed process admits a semimartingale structure that supports arbitrage-free valuation within its natural filtration. Therefore, we work under a risk-neutral measure and use the corresponding pricing PDE formulation for the option value.

Here H, α, and β are not varied. The choice $H = 0.85$ determines the time-dependent fractional contribution to the diffusion coefficient, while α and β determine the relative size of the Brownian and fractional components. Earlier MFBM computations show that changing these parameters can alter both option values and numerical convergence [12], [13]. The comparisons reported here therefore apply to $H = 0.85$ and $\alpha = \beta = 1$; they are not intended as a sensitivity study over the MFBM parameter space.

From the MFBM dynamics in Equation (1), the option price $V(S,t)$ under the risk-neutral measure satisfies the Black-Scholes type PDE in Equation (2) with a time-dependent effective diffusion coefficient [14], [25] :

$$\frac{\partial V}{\partial t} + \frac{1}{2}\sigma^2(\alpha^2 + 2H\beta^2 t^{2H-1})S^2\frac{\partial^2 V}{\partial S^2} + rS\frac{\partial V}{\partial S} - rV = 0, \qquad S \in (S_{min}, S_U),\ t \in (0,T). \tag{2}$$

For $\alpha = \beta = 1$, the diffusion coefficient term in Equation (2) simplifies as shown in Equation (3):

$$\frac{1}{2}\sigma^2(1 + 2Ht^{2H-1}) = \frac{1}{2}\sigma^2 + H\sigma^2 t^{2H-1}. \tag{3}$$

The contract analyzed is an up-and-out call option with strike K and upper barrier S_U. The terminal payoff is defined in Equation (4):

$$V(S,T) = max(S-K,0)\,\mathbf{1}_{\{S<S_U\}}. \tag{4}$$

We assume a continuously monitored up-and-out barrier; therefore, the knock-out feature is enforced by an absorbing (Dirichlet) boundary condition at S_U for all $t \in [0,T]$, given in Equation (5):

$$V(S_U,t) = 0, \qquad t \in [0,T]. \tag{5}$$

The spatial domain is truncated at the lower boundary $S_{\min} = 10^{-4}K$ and the lower boundary condition is imposed as in Equation (6):

$$V(S_{min}, t) = 0, \qquad t \in [0, T], \tag{6}$$

so that the computational domain is $S \in [S_{\min}, S_U]$.

Unless otherwise stated, the numerical experiments use $S_0 = 1000, K = 1000, S_U = 1200, r = 0.05,$ and $T = 0.5$. We set $\alpha = \beta = 1$ and $H = 0.85$, and consider three volatility regimes $\sigma \in \{0.2, 0.4, 0.6\}$. Dividends are ignored ($q = 0$). The lower truncation is $S_{\min} = 10^{-4}K$, so the computational domain is $S \in [S_{\min}, S_U]$, equivalently $x \in [\ln(S_{\min}), \ln(S_U))$ in log-space.

The numerical configuration is representative but stylized and is not calibrated to a particular traded contract. With the initial asset price and strike both set at 1000 and the upper barrier at 1200, the barrier is 20% above the initial level. This keeps the option active initially while retaining a barrier that is numerically relevant over the six-month maturity. The three volatility levels are used to examine whether the time-stepping behavior changes as diffusion becomes stronger.

To march forward in time, we work with the remaining time to maturity $\tau = T - t$, so the solution is computed from $\tau = 0$ (maturity) to $\tau = T$ (initial time). Next, we apply the log transformation $x = \ln S$ and the discounting transformation defined in Equation (7):

$$U(x, \tau) = e^{r\tau} V(e^x, T - \tau). \tag{7}$$

with $x \in [x_L, x_U] = [\ln(S_{\min}), \ln(S_U)]$, the PDE in Equation (2) transforms into the one-dimensional convection diffusion equation given in Equation (8):

$$\frac{\partial U}{\partial \tau} = a(\tau)\frac{\partial^2 U}{\partial x^2} + b(\tau)\frac{\partial U}{\partial x}, \tag{8}$$

The time-dependent coefficients in Equation (8) are defined in Equations (9) and (10):

$$a(\tau) = \frac{1}{2}\sigma^2 + H\sigma^2 (T - \tau)^{2H-1}, \tag{9}$$

$$b(\tau) = r - a(\tau), \tag{10}$$

The initial condition at $\tau = 0$ is specified in Equation (11):

$$U(x, 0) = max(e^x - K, 0), \tag{11}$$

and the boundary conditions for all $\tau \in [0, T]$ are given in Equations (12) and (13):

$$U(x_L, \tau) = 0, \tag{12}$$

$$U(x_U, \tau) = 0. \tag{13}$$

The spatial discretization uses a uniform grid defined in Equation (14):

$$x_j = x_L + j\Delta x, \qquad j = 0,1, \dots, N_x, \tag{14}$$

with mesh width defined in Equation (15):

$$\Delta x = \frac{x_U - x_L}{N_x}. \tag{15}$$

The solution is computed at interior nodes $j = 1, \dots, N_x - 1$. The first and second derivatives are approximated by second-order central differences in Equations (16) and (17):

$$U_x(x_j, \tau_n) \approx \frac{U_{j+1}^n - U_{j-1}^n}{2\Delta x}, \tag{16}$$

$$U_{xx}(x_j, \tau_n) \approx \frac{U_{j+1}^n - 2U_j^n + U_{j-1}^n}{\Delta x^2}. \tag{17}$$

Thus, the spatial operator at time τ_n can be written as a tridiagonal operator $A(\tau_n)$ with coefficients given in Equations (18) to (20):

$$c_L(\tau_n) = \frac{a(\tau_n)}{\Delta x^2} - \frac{b(\tau_n)}{2\Delta x}, \tag{18}$$

$$c_D(\tau_n) = -\frac{2a(\tau_n)}{\Delta x^2}, \tag{19}$$

$$c_U(\tau_n) = \frac{a(\tau_n)}{\Delta x^2} + \frac{b(\tau_n)}{2\Delta x}. \tag{20}$$

For time integration, we use the θ scheme written in Equation (21):

$$\big(I - \theta \Delta\tau\, A(\tau_{n+1})\big)U^{n+1} = U^n + (1-\theta)\Delta\tau\, A(\tau_n)U^n, \qquad n = 0,1,\dots,N_t - 1, \tag{21}$$

with $\Delta\tau = T/N_t$.
Three schemes were compared:

a. IMPL (Implicit Backward Euler): $\theta = 1$ (first-order in time).
b. CN (Crank-Nicolson): $\theta = \frac{1}{2}$ (second-order for sufficiently regular solutions).
c. CN-R (Crank-Nicolson + Rannacher start-up): replaces the first m Crank-Nicolson steps with $2m$ Backward Euler half steps of size $\Delta\tau/2$, and then continues with Crank-Nicolson; in the experiments, $m = 2$.

All numerical experiments were implemented in Python using NumPy for array computations and Matplotlib for visualization. At each time step, the tridiagonal linear system was solved using the banded solver scipy.linalg.solve_banded. The same solver was used for all schemes to ensure comparable linear solve costs [26].

The price at the evaluation point S_0 is obtained by linear interpolation on the log-price grid around $x_0 = \ln(S_0)$, and then discounted to obtain the initial time price given by Equation (22):

$$V(S_0, 0) = e^{-rT}U(x_0, T). \tag{22}$$

Thus, for each time resolution N_t, we obtain $P(N_t) \equiv V(S_0, 0)$.

Since analytical solutions for up-and-out call configurations under MFBM are not available in practical closed form, accuracy is measured relative to a discrete reference solution P_{ref}, defined as the value produced by the CN-R scheme on a very fine time grid $N_t^{\text{ref}} = 65536$ with $N_x = 8192$. The relative error at the evaluation point is defined by Equation (23):

$$RelErr(N_t) = \frac{|\, P(N_t) - P_{ref} \,|}{|\, P_{ref} \,|}. \tag{23}$$

The benchmark uses CN-R with 65,536 time steps on the same spatial grid ($N_x = 8{,}192$). As a practical adequacy check, the CN-R solution at 16,384 time steps differs from this benchmark by less than 1.4e-8 in relative terms across the three volatility regimes (Tables 1-3), far below the errors observed on coarse and moderate grids. The benchmark is therefore used only as a high-resolution within-study reference; it does not remove the remaining spatial-discretization error. Using a high-resolution numerical solution as a benchmark is consistent with established benchmarking practice in computational option pricing [27].

Global stability is evaluated through undershoot diagnostics $\min(U)$, defined by Equation (24) as the minimum value of the solution over all interior points and all time levels:

$$min(U) = \min_{0\leq n\leq N_t} \min_{1\leq j\leq N_x-1} U_j^n. \tag{24}$$

Since $\min(U)$ is a global minimum throughout the time-marching process, a negative value indicates that undershoot has occurred at some stage even if the final time solution becomes non-negative again. With the transformation in Equation (7) and $e^{r\tau} > 0$, the condition $\min(U) < 0$ is equivalent to having $V < 0$ somewhere on the grid, which is not expected for claims with non-negative payoffs [24].

Time convergence tests are performed by fixing the spatial grid at $N_x = 8192$ and varying the number of time steps $N_t = 2^k$ for $k = 3, \ldots, 15$, under three volatility regimes $\sigma \in \{0.2, 0.4, 0.6\}$ with other parameters fixed. For each scheme-regime combination and each N_t, we report $P(N_t)$, $\mathrm{RelErr}(N_t)$, $\min(U)$, and the wall-clock execution time measured using time.perf_counter() for the core computation excluding post-processing.

Fixing the spatial grid at $N_x = 8{,}192$ is a deliberate experimental design choice: it isolates temporal discretization effects so that the three time-stepping schemes can be compared under the same spatial error. Consequently, the study does not claim full space-time convergence; joint spatial and temporal refinement is outside the present scope.

The MFBM parameters other than σ are kept at $H = 0.85$ and $\alpha = \beta = 1$. Every run was made on the same Intel Core i7-1165G7 2.80 GHz computer with 16 GB RAM and 64-bit Windows. For that reason, the recorded times are used only to compare the three schemes within this experiment; they are not intended as hardware-independent benchmarks.

Several limitations of the numerical setup should be noted. The time-refinement experiments were performed on a fixed spatial grid and a fixed truncated domain, so the reported trends primarily characterize temporal discretization effects conditional on the chosen spatial resolution and boundaries; a full space–time refinement study is beyond the present scope. The barrier was assumed continuously monitored, and the results may differ under discrete monitoring, which typically requires additional corrections. Model parameters were restricted to a semimartingale-admissible MFBM setting (with fixed weights and Hurst parameter), and different parameter ranges may change the quantitative behavior. Since closed-form solutions for the considered MFBM barrier configuration are unavailable, accuracy was assessed against a numerical reference solution computed on a much finer time grid; therefore, errors should be interpreted as relative to this benchmark. Finally, reported runtimes depend on the specific hardware/software environment and are intended for consistent within-study comparisons across schemes.

3. RESULT AND ANALYSIS

This section reports the numerical behavior of IMPL, CN, and CN-R using relative error to the high-resolution reference price, the global minimum min(U), and runtime. To distinguish numerical evidence from interpretation, Section 3.1 first summarizes the table and figure results, while Section 3.2 discusses their implications for stability, computational cost, and practical use.

3.1 Numerical results

Because the spatial grid is fixed at N_x = 8,192 in all experiments, the runtime changes reported below primarily reflect temporal refinement; the implications of changing spatial resolution are discussed in Section 3.2.

Tables 1–3 report representative results for three time-resolution phases, $N_t = 8$ (very coarse), $N_t = 128$ (transitional), and $N_t = 16384$ (fine/near asymptotic), for each volatility regime. For each scheme and N_t, the tables list the computed option price, the relative error with respect to the reference price P_{ref}, the global undershoot diagnostic $\min(U)$, and the runtime.

Table 1. Time-convergence and stability diagnostics with runtime for σ = 0.2.

Scheme	N_t	Price	$RelErr(N_t)$	$\min(U)$	Runtime(s)
IMPL	8	15.951	1.24×10^{-1}	≈ 0	2.34×10^{-3}
CN	8	9.845	3.06×10^{-1}	-2.82×10^{2}	3.83×10^{-3}
CN-R	8	14.426	1.63×10^{-2}	≈ 0	4.59×10^{-3}
IMPL	128	14.309	8.13×10^{-3}	≈ 0	4.89×10^{-3}
CN	128	14.128	4.66×10^{-3}	-1.54×10^{2}	6.45×10^{-2}
CN-R	128	14.195	8.20×10^{-5}	≈ 0	7.83×10^{-2}
IMPL	16384	14.195	6.36×10^{-5}	≈ 0	6.33×10^{0}
CN	16384	14.194	3.31×10^{-9}	≈ 0	5.88×10^{0}
CN-R	16384	14.194	8.90×10^{-9}	≈ 0	5.86×10^{0}

Table 2. Time-convergence and stability diagnostics with runtime for σ = 0.4.

Scheme	N_t	Price	$RelErr(N_t)$	$\min(U)$	Runtime(s)
IMPL	8	3.385	2.93×10^{-1}	≈ 0	3.92×10^{-3}
CN	8	-5.648	3.16×10^{0}	-3.05×10^{2}	4.21×10^{-3}
CN-R	8	2.679	2.39×10^{-2}	≈ 0	4.87×10^{-3}
IMPL	128	2.658	1.59×10^{-2}	≈ 0	5.47×10^{-2}
CN	128	2.241	1.44×10^{-1}	-1.77×10^{2}	5.33×10^{-2}
CN-R	128	2.617	1.20×10^{-4}	≈ 0	5.30×10^{-2}
IMPL	16384	2.617	1.22×10^{-4}	≈ 0	8.79×10^{0}
CN	16384	2.617	1.69×10^{-9}	≈ 0	9.34×10^{0}
CN-R	16384	2.617	1.25×10^{-8}	≈ 0	9.35×10^{0}

Table 3. Time-convergence and stability diagnostics with runtime for σ = 0.6.

Scheme	N_t	Price	$RelErr(N_t)$	$\min(U)$	Runtime(s)
IMPL	8	1.115	3.51×10^{-1}	≈ 0	2.13×10^{-3}
CN	8	-10.004	1.31×10^{1}	-3.13×10^{2}	1.94×10^{-3}
CN-R	8	0.845	2.31×10^{-2}	≈ 0	2.36×10^{-3}
IMPL	128	0.841	1.80×10^{-2}	≈ 0	5.67×10^{-2}
CN	128	0.138	8.33×10^{-1}	-1.85×10^{2}	4.01×10^{-2}
CN-R	128	0.826	1.28×10^{-4}	≈ 0	4.14×10^{-2}
IMPL	16384	0.826	1.39×10^{-4}	≈ 0	6.67×10^{0}
CN	16384	0.826	1.12×10^{-9}	-4.90×10^{1}	7.14×10^{0}
CN-R	16384	0.826	1.34×10^{-8}	≈ 0	7.18×10^{0}

Note for Tables 1-3: nonnegative min(U) values with magnitude below 10^{-12} are reported as ≈0 because they are at numerical round-off level.

Tables 1-3 show the largest instability for standard CN on coarse time grids. At 8-time steps, CN produces prices of 9.845, -5.648, and -10.004 for $\sigma = 0.2$, 0.4, and 0.6, respectively, while the corresponding global minima are -282, -305, and -313. IMPL and CN-R do not show comparable negative undershoots at this resolution.

At 128-time steps, CN-R yields relative errors of 0.0000820, 0.000120, and 0.000128 with $\min(U)$ effectively zero and runtimes of 0.0783, 0.0530, and 0.0414 s. At the same resolution, IMPL errors are 0.00813, 0.0159, and 0.0180, whereas CN errors are 0.00466, 0.144, and 0.833 and CN retains large negative minima. Thus, a target relative error of 0.001 is reached by CN-R in all three regimes at 128-time steps, but not by IMPL or standard CN at this representative resolution.

For σ = 0.4, CN-R at $N_t = 128$ achieved a relative error of 0.000120 in 0.0530 s, essentially matching IMPL at $N_t = 16{,}384$ (0.000122 in 8.79 s). Thus, in this experiment, CN-R used 1/128 as many time steps and about 1/166 of the runtime for comparable accuracy.

At 16,384-time steps, point prices from all three schemes are close to the reference price. However, CN at $\sigma = 0.6$ still records $\min(U) = -49.0$ despite a pointwise relative error of 1.12e-9, whereas CN-R has $\min(U) = 0$. This numerical contrast shows that pointwise price convergence and global non-negativity need not occur simultaneously.

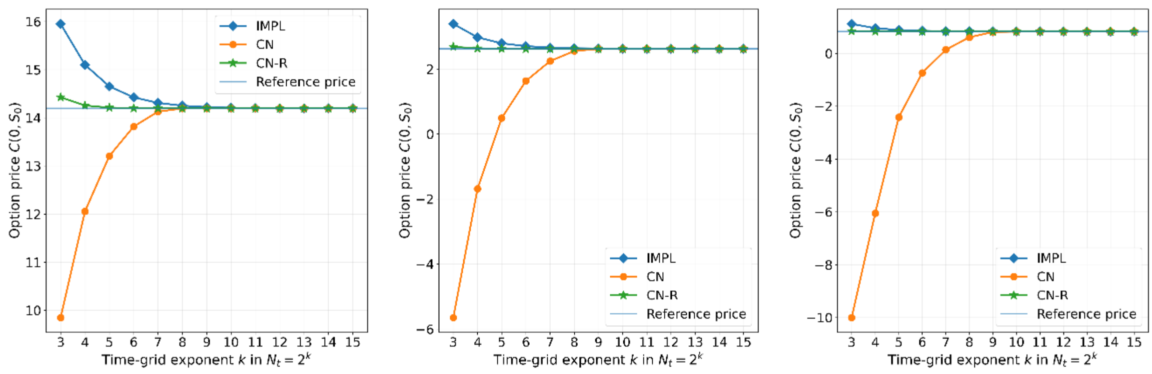

(a) (b) (c)

Figure 1. Time convergence: option prices against N_t for (a) low σ, (b) mid σ, (c) high σ; $N_x = 8192$, dotted lines indicate P_{ref}.

The separation among the methods is easiest to see at small k in Figure 1. For σ = 0.4 and 0.6, the first CN prices lie well away from the reference and move toward it only after several refinements. CN-R is close much earlier. IMPL approaches the same limiting price more gradually.

The minimum-value curves in Figure 2 add information that is not visible from the price at S_0 alone. CN is negative somewhere on the grid through much of the coarse and intermediate range, and the negative excursion disappears only after further refinement. CN-R stays essentially at zero throughout the tested range, while IMPL also avoids the large negative excursions.

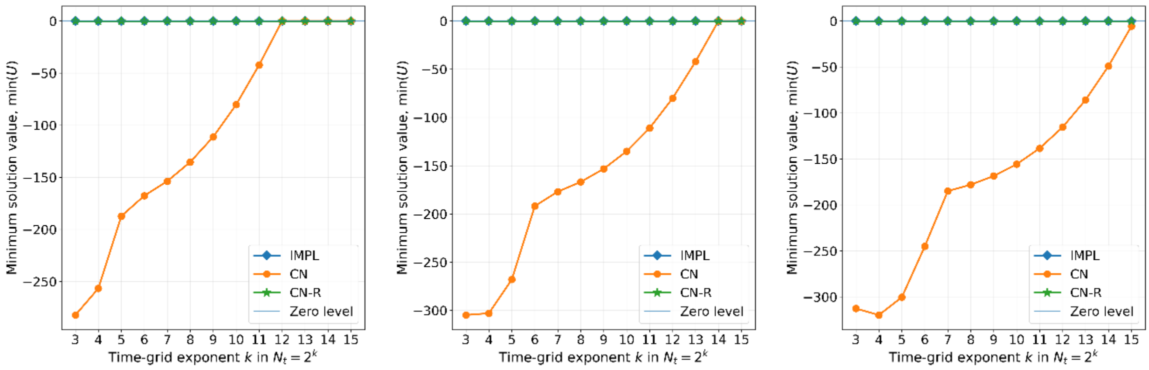

(a) (b) (c)

Figure 2. Diagnostic undershoot: $\min(U)$ during time-marching $N_t = 2^k$ for (a) low σ, (b) mid σ, and (c) high σ at N_x fixed.

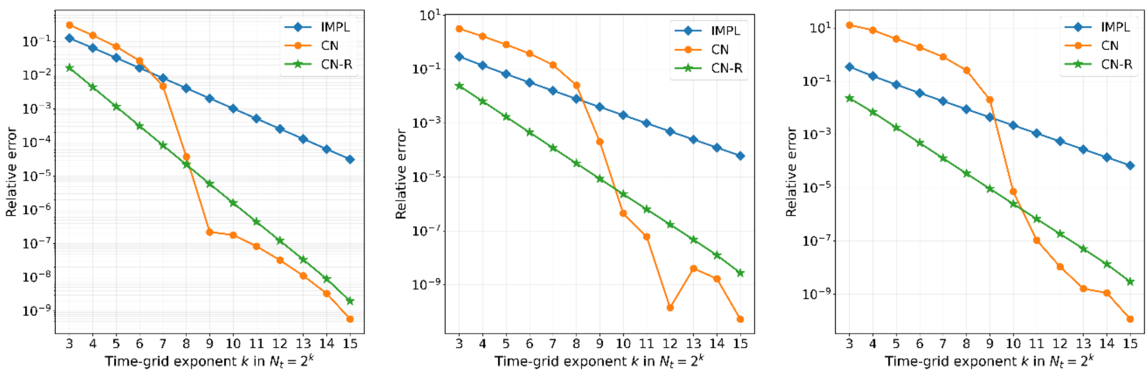

(a) (b) (c)

Figure 3. Relative error versus k for $N_t = 2^k$ under (a) low σ, (b) mid σ, and (c) high σ; comparison of IMPL, CN, and CN-R with respect to fixed P_{ref} at fixed N_x.

Figure 3 shows how these differences appear in the error sequence. IMPL decreases in a fairly regular but comparatively slow manner. CN has a long pre-asymptotic region, followed by a sharp drop once the time grid is sufficiently fine. CN-R begins that decline earlier and does so more smoothly. On the finest grids, the slopes are compatible with first-order time behavior for Backward Euler and second-order behavior for the Crank-Nicolson schemes. Since Nx is not refined, this statement concerns temporal behavior only.

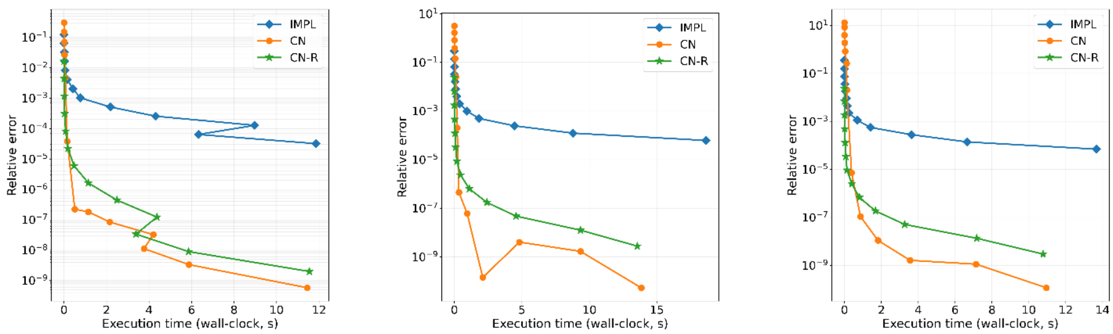

(a) (b) (c)

Figure 4. Relative error versus execution time for IMPL, CN, and CN-R at (a) low σ, (b) mid σ, and (c) high σ, with constant N_x.

Figure 4 gives the same comparison against measured computing time rather than Nt. CN-R reaches the low-error part of the plot at relatively modest runtimes. IMPL pays a larger time cost for the same reduction in error because of its slower temporal convergence. Standard CN eventually produces very small pointwise errors, but those points occur only after the oscillatory phase seen on coarser grids has largely disappeared.

3.2 Discussion

The numbers at $N_t = 128$ already separate the three methods. CN-R gives relative errors of 8.20×10^{-5}, 1.20×10^{-4}, and 1.28×10^{-4} for $\sigma = 0.2$, 0.4, and 0.6, whereas IMPL and CN are not below 10^{-3} in all three cases. A second result is more important for stability. At $\sigma = 0.6$ and $N_t = 16{,}384$, CN has a pointwise error of 1.12×10^{-9} at S_0, but $\min(U)$ is -49. Thus, agreement at S0 does not guarantee a non-negative solution over the grid.

Rannacher smoothing acts only at the beginning of the time march. Its Backward Euler half steps attenuate the oscillatory components associated with the nonsmooth terminal condition before the CN updates start [22], [23]. Figures 1-3 reflect this difference: the CN-R curve enters the small-error region sooner, whereas standard CN remains in its oscillatory phase for more refinement levels, particularly when σ is larger.

Deswal and Kumar [28] reported a closely related effect for option problems with nonsmooth initial data: standard Crank-Nicolson lost its expected quadratic convergence and developed spurious oscillations, while Rannacher time-marching restored the expected behavior.

The reported runtimes have a limited interpretation. Nx is fixed at 8,192, so adding a time level means solving one more tridiagonal system of exactly the same dimension. The timing curves therefore describe temporal refinement on the machine used in this study, not a hardware-independent speed comparison. At Nt = 128, however, the three methods share the same spatial grid, machine, and number of time steps, which makes their contrast directly comparable.

The parameter values in the present experiment were selected for a controlled numerical comparison. Discrete monitoring, transaction costs, jumps, time-varying volatility, or different choices of H and the mixing weights would define a different test problem. Joint space-time refinement and those model variations remain to be examined. A direct comparison with Monte Carlo methods or alternative PDE solvers is beyond the present scope, because this study is designed specifically to isolate time-stepping effects within a common finite-difference spatial framework.

Recent studies illustrate why these extensions should be treated as separate numerical problems. Ma et al. [29] obtained a different PIDE after introducing illiquidity and jumps into an MFBM option model. Huang and Luo [30] treated discretely monitored single and double barrier options with a numerical method built around the monitoring dates.

4. CONCLUSION

Once the time grid is very fine, the three schemes give nearly the same value at S_0. Their behavior before that stage is quite different. Backward Euler damps the oscillation from the start, but its error falls slowly. CN becomes extremely accurate after sufficient refinement, although large negative excursions can persist on coarser grids. In the present tests, CN-R suppresses those excursions and is already at roughly 10^{-4} relative error when $Nt = 128$ for each volatility level. Thus, under the numerical configuration examined here, CN-R provides the most reliable balance among accuracy, global stability, and computational cost when only a moderate number of time steps is practical.

This conclusion is tied to the numerical experiment rather than to all MFBM barrier problems. It concerns one barrier specification, $N_x = 8{,}192$, continuous monitoring, $H = 0.85$, $\alpha = \beta = 1$, and a numerical reference value. Claims beyond that setting require additional checks, especially joint refinement in space and time and tests with other MFBM and barrier parameters.

For routine barrier-option pricing under the stated MFBM setting, practitioners should therefore favor Crank-Nicolson with a Rannacher start-up (CN-R) when a moderate time grid must balance accuracy, global non-negativity, and runtime.

ACKNOWLEDGMENT

The author gratefully acknowledges Universitas Sanata Dharma through the Institute for Research and Community Service (LPPM) for financial support under the 2022 Regular/General Research Scheme. This article was developed from the funded research project on barrier option pricing under mixed fractional Brownian motion using finite-difference methods.

5. REFERENCES

[1] M. Broadie, P. Glasserman, and S. Kou, "A Continuity Correction for Discrete Barrier Options," *Math. Financ.*, vol. 7, no. 4, pp. 325–349, Oct. 1997, https://doi.org/10.1111/1467-9965.00035
[2] H. Geman and M. Yor, "Pricing and hedging double-barrier options: A probabilistic approach," *Math. Financ.*, vol. 6, no. 4, 1996, https://doi.org/10.1111/j.1467-9965.1996.tb00122.x
[3] N. Kunitomo and M. Ikeda, "Pricing Options With Curved Boundaries," *Math. Financ.*, vol. 2, no. 4, 1992, https://doi.org/10.1111/j.1467-9965.1992.tb00033.x
[4] R. Zvan, K. R. Vetzal, and P. A. Forsyth, "PDE methods for pricing barrier options," *J. Econ. Dyn. Control*, vol. 24, no. 11–12, pp. 1563–1590, Oct. 2000, https://doi.org/10.1016/S0165-1889(00)00002-6
[5] L. V. Ballestra, "Enhancing finite difference approximations for double barrier options: mesh optimization and repeated Richardson extrapolation," *Computational Management Science*, vol. 18, no. 2, pp. 239–263, Jun. 2021, https://doi.org/10.1007/s10287-021-00394-9
[6] F. Comte and E. Renault, "Long memory in continuous-time stochastic volatility models," *Math. Financ.*, vol. 8, no. 4, pp. 291–323, Oct. 1998, https://doi.org/10.1111/1467-9965.00057
[7] B. B. Mandelbrot and J. W. Van Ness, "Fractional Brownian Motions, Fractional Noises and Applications," *SIAM Review*, vol. 10, no. 4, 1968, https://doi.org/10.1137/1010093
[8] P. Cheridito, "Arbitrage in fractional Brownian motion models," *Finance and Stochastics*, vol. 7, no. 4, 2003, https://doi.org/10.1007/s007800300101
[9] L. C. G. Rogers, "Arbitrage with Fractional Brownian Motion," *Math. Financ.*, vol. 7, no. 1, pp. 95–105, Jan. 1997, https://doi.org/10.1111/1467-9965.00025
[10] P. Cheridito, "Mixed fractional Brownian motion," *Bernoulli*, vol. 7, no. 6, pp. 913–934, 2001, https://doi.org/10.2307/3318626
[11] S. Rostek and R. Schöbel, "A note on the use of fractional Brownian motion for financial modeling," *Econ. Model.*, vol. 30, no. 1, 2013, https://doi.org/10.1016/j.econmod.2012.09.003
[12] C. E. Murwaningtyas, S. H. Kartiko, G. Gunardi, and H. P. Suryawan, "Finite Difference Method for Pricing of Indonesian Option under a Mixed Fractional Brownian Motion," *Mathematics and Statistics*, vol. 8, no. 5, pp. 610–619, Sep. 2020, https://doi.org/10.13189/ms.2020.080516
[13] Y. Wang and J. Wang, "Pricing of American Carbon Emission Derivatives and Numerical Method under the Mixed Fractional Brownian Motion," *Discrete Dyn. Nat. Soc.*, vol. 2021, no. 1, p. 6612284, Jan. 2021, https://doi.org/10.1155/2021/6612284
[14] L. V. Ballestra, G. Pacelli, and D. Radi, "A very efficient approach for pricing barrier options on an underlying described by the mixed fractional Brownian motion," *Chaos Solitons Fractals*, vol. 87, pp. 240–248, Jun. 2016, https://doi.org/10.1016/j.chaos.2016.04.008
[15] B. Ji, X. Tao, and Y. Ji, "Barrier Option Pricing in the Sub-Mixed Fractional Brownian Motion with Jump Environment," *Fractal and Fractional*, vol. 6, no. 5, 2022, https://doi.org/10.3390/fractalfract6050244
[16] M. Rezaei, "The valuation of double barrier options under mixed fractional Brownian motion model with transaction costs," Dec. 2023, https://doi.org/10.21203/RS.3.RS-3719661/V1
[17] D. Yan, X. J. Huang, G. Ma, and X. J. He, "Pricing American options with exogenous and endogenous transaction costs," *Computers & Mathematics with Applications*, vol. 200, pp. 85–101, Dec. 2025, https://doi.org/10.1016/J.CAMWA.2025.09.008
[18] W. Zhang, G. He, B. Q. Hu, and H. Liu, "Fuzzy Pricing of Barrier Options with Jump Diffusion Mixed Fractional Brownian Motion," *International Journal of Fuzzy Systems*, vol. 28, no. 5, pp. 1533–1556, 2026 (published online Apr. 22, 2025), https://doi.org/10.1007/s40815-025-02037-6
[19] O. Østerby, "Five ways of reducing the Crank-Nicolson oscillations," *BIT Numer. Math.*, vol. 43, no. 4, pp. 811–822, Dec. 2003, https://doi.org/10.1023/B:BITN.0000009942.00540.94
[20] D. M. Pooley, K. R. Vetzal, and P. A. Forsyth, "Convergence remedies for non-smooth payoffs in option pricing," *The Journal of Computational Finance*, vol. 6, no. 4, pp. 25–40, Jun. 2003, https://doi.org/10.21314/JCF.2003.101
[21] N. Umeorah and P. Mashele, "A Crank-Nicolson finite difference approach on the numerical estimation of rebate barrier option prices," *Cogent Economics & Finance*, vol. 7, no. 1, p. 1598835, Jan. 2019, https://doi.org/10.1080/23322039.2019.1598835
[22] M. B. Giles and R. Carter, "Convergence analysis of Crank–Nicolson and Rannacher time-marching," *The Journal of Computational Finance*, vol. 9, no. 4, pp. 89–112, 2006, https://doi.org/10.21314/JCF.2006.152
[23] R. Rannacher, "Finite element solution of diffusion problems with irregular data," *Numer. Math. (Heidelb).*, vol. 43, no. 2, pp. 309–327, Jun. 1984, https://doi.org/10.1007/BF01390130
[24] J. M. Harrison and S. R. Pliska, "Martingales and stochastic integrals in the theory of continuous trading," *Stoch. Process. Their Appl.*, vol. 11, no. 3, pp. 215–260, 1981, https://doi.org/10.1016/0304-4149(81)90026-0
[25] F. Shokrollahi and A. Klçman, "Pricing currency option in a mixed fractional Brownian motion with jumps environment," *Math. Probl. Eng.*, vol. 2014, 2014, https://doi.org/10.1155/2014/858210

[26] P. Virtanen *et al.*, "SciPy 1.0: fundamental algorithms for scientific computing in Python," *Nat. Methods*, vol. 17, no. 3, pp. 261–272, Mar. 2020, https://doi.org/10.1038/s41592-019-0686-2
[27] L. von Sydow *et al.*, "BENCHOP – The BENCHmarking project in option pricing," *Int. J. Comput. Math.*, vol. 92, no. 12, pp. 2361–2379, Dec. 2015, https://doi.org/10.1080/00207160.2015.1072172
[28] K. Deswal and D. Kumar, "Rannacher time-marching with orthogonal spline collocation method for retrieving the discontinuous behavior of hedging parameters," *Appl. Math. Comput.*, vol. 427, p. 127168, Aug. 2022, https://doi.org/10.1016/J.AMC.2022.127168
[29] P. Ma, M. Taghipour, and C. Cattani, "Option pricing in the illiquid markets under the mixed fractional Brownian motion model," *Chaos Solitons Fractals*, vol. 182, p. 114806, May 2024, https://doi.org/10.1016/J.CHAOS.2024.114806
[30] M. Huang and G. Luo, "A simple and efficient numerical method for pricing discretely monitored early-exercise options," *Appl. Math. Comput.*, vol. 422, p. 126985, Jun. 2022, https://doi.org/10.1016/J.AMC.2022.126985